IEEE Photonics Journal
An IEEE Photonics Society Publication

Open Access

Comparison of Anisotropy Reduction Strategies for Transformation Optics Designs

Volume 7, Number 1, February 2015

M. A. F. C. Junqueira
L. H. Gabrielli
D. H. Spadoti

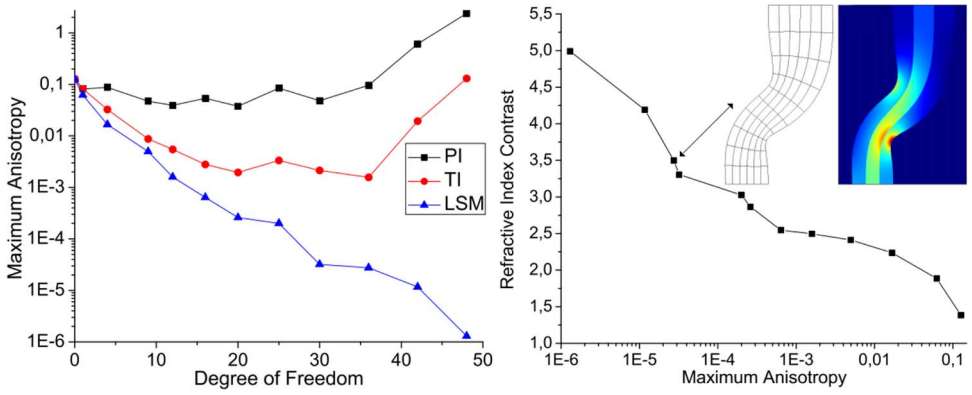

DOI: 10.1109/JPHOT.2015.2396008
1943-0655

IEEE photonics SOCIETY

IEEE

Comparison of Anisotropy Reduction Strategies for Transformation Optics Designs

M. A. F. C. Junqueira,[1] L. H. Gabrielli,[2] and D. H. Spadoti[1]

[1]Institute of Systems Engineering and Information Technology, Federal University of Itajubá, 37500-903 Itajubá, Brazil
[2]School of Electrical and Computer Engineering, University of Campinas, 13083-970 Campinas, Brazil

DOI: 10.1109/JPHOT.2015.2396008

Manuscript received November 18, 2014; revised December 29, 2014; accepted January 7, 2015. Date of publication January 22, 2015; date of current version February 10, 2015. This work was supported by CNPq, CAPES, and FAPEMIG. Corresponding author: M. A. F. C. Junqueira (e-mail: mateusafcj@gmail.com).

Abstract: In this paper, we present new strategies to reduce anisotropy in transformation optics designs and compare them to other techniques. Perturbation functions are used to modify the original transformation to achieve a quasi-conformal map, resulting in a medium with isotropic properties. All strategies investigated have no effect on the original boundary conditions of the transformation, such that neither the initial design is affected nor are reflections at the boundaries introduced. The results show that there exists a clear compromise between the residual anisotropy and the required refractive index contrast in the optimized transformation, but the former can be made as small as desired when the degree of freedom provided by perturbation functions is increased, although it is never exactly zero.

Index Terms: Transformation optics, quasi-conformal mapping, waveguides, integrated optics, waveguide circuits, metamaterials, least squares method, polynomial and trigonometric series.

1. Introduction

The Transformation Optics (TO) [1]–[5] technique has proved to be a powerful tool for the creation of new optical devices. Its power comes from the great freedom in designing electromagnetic functionalities by merely using coordinate system deformation, which is reflected in a deformation of the electromagnetic space and physically implemented through well-defined permittivity and permeability tensors. Thus, to make use of TO, one must describe the desired behavior of the light paths in terms of a coordinate transformation and calculate the required material parameters that provide functionality. This process, however, usually results in inhomogeneous and highly anisotropic materials requirements, which, in practice, are extremely hard to be achieved. To minimize this issue, researchers have proposed the use of *quasi-conformal* mappings [6], [7], which minimize the anisotropy in the original coordinate transformation.

The TO formalism is based on the invariance of Maxwell's equations over space-time coordinate transformations. In particular, for a spacial transformation with metric tensor "*g*," the

transformed medium properties, i.e., ε' is the electric permittivity, and μ' is the magnetic permeability, are given by [8]

$$\varepsilon'^{ij} = \varepsilon\sqrt{g}g^{ij} \tag{1}$$

$$\mu'^{ij} = \mu\sqrt{g}g^{ij}. \tag{2}$$

According to those expressions, the transformed medium will be isotropic only when the underlying coordinate transformation is conformal, i.e., a transformation for which the Cauchy-Riemann equations are satisfied [9]:

$$\frac{\partial x'}{\partial x} = \frac{\partial y'}{\partial y} \tag{3}$$

$$\frac{\partial x'}{\partial y} = -\frac{\partial y'}{\partial x}. \tag{4}$$

There are some methods to achieve quasi-conformal maps, which have reduced deviations in the Cauchy-Riemann equations (3) and (4), using non-linear optimization and minimization with sliding boundary conditions [7], [10], [11]. Practical devices with quasi-conformal mapping, such as: bends waveguides, expander, lenses and antennas can be seen in [10]–[20].

In this paper, in order to reduce anisotropy, we use a parameterization technique to approximate quasi-conformal transformations. Polynomial and trigonometric inversions are proposed and these techniques are compared to the Least Squares Method (LSM) from [17]. The inversions can be used to achieve exact isotropy in a few sampling points of the transformed region. Besides, one could also employ the trigonometric series instead of the polynomial in the LSM. Additionally, it was verified that the required refractive index contrast to fabricate the final media increases with the desired level of anisotropy reduction. Two devices are designed, optimized and simulated to support our analysis.

Our general approach to minimize anisotropy in the transformation is to sample the original medium defining a set of points S and then apply the minimization technique at those points. To be able to modify the anisotropy, the original (anisotropic) transformation must include the necessary degrees of freedom allowing the minimization of error in (3) and (4). The transformation has been chosen to be written as

$$x' = f_x(x, y) + b(x, y)P_x(x, y) \tag{5}$$

$$y' = f_y(x, y) + b(x, y)P_y(x, y) \tag{6}$$

where x' and y' are the new coordinates, and f_x and f_y represent the original transformation. The necessary degrees of freedom for the minimization are included in P_x and P_y, which are perturbation functions written in finite series forms. The function b is a helper function that overrides the effect of the power series at the boundaries of the original transformation, i.e., $b(x, y) = 0$ on specific boundaries. The transformation value at these boundaries (original boundary conditions) determine the functionality of the TO device and should, most of the time, ensure minimal reflections between the device and the external media [10], [21], [22]. Therefore, it is desirable that the anisotropy minimization technique does not modify those boundaries conditions, leading to our definition of b.

The transformation shows no reflection at a given boundary if, and only if, it is continuous with the external coordinate system at that boundary [10]. However, this condition can only be exactly met by the identity transformation due to the uniqueness theorem [9] as discussed in [1], [17]. It is possible, however, to minimize reflections by approximating the identity transformation close to the boundaries at the price of acceptable levels of anisotropy.

Combining the Jacobian of the transformation defined in (5) and (6) with the conditions imposed in (3) and (4), a linear system in the coefficients of the series P_x and P_y are obtained. If the same number of sampling points are used as coefficients in the series, the system can be readily inverted and a transformation is found, which is exactly isotropic at the sampling points.

However, residual anisotropy remains between those points, representing the non-conformity of the transformation and a possible source of performance degradation in the final device.

This technique does not allow direct control among the interpolated points, therefore it can still result in elevated anisotropy in specific locations. As indicated in [10], the maximum anisotropy has greater importance in the device performance than its average anisotropy, and thus, it should be reduced. For that reason, a representation with smoother basis functions can be used for the series, such as sines and cosines. This choice is shown to indeed reduce the maximum anisotropy in the interpolated points with a numerical example in Section 2.

Additionally, it is also possible to over-specify the linear system by including a larger number of sampled points. In this case, it is possible to use the LSM to reduce the deviation in (3) and (4) using the error function

$$E = \sum_{S} \left[\left(\frac{\partial x'}{\partial x} - \frac{\partial y'}{\partial y} \right)^2 + \left(\frac{\partial x'}{\partial y} + \frac{\partial y'}{\partial x} \right)^2 \right]. \tag{7}$$

Details of the implementation of the LSM applied to TO can be found in [17], where it is also demonstrated that the choice of S allows the reduction of the ratio between the maximum and the average anisotropy.

In this work, the results of both direct inversion methods (with polynomial and trigonometric series) and the LSM are compared, to show that the choice of smoother basis functions indeed improve the final design, but the use of the LSM is still more effective in reducing the maximum anisotropy even with a polynomial basis. To quantify the residual anisotropy in the transformed medium we use the measure [23]

$$K = \frac{1 + |\nu|^2}{1 - |\nu|^2} = \mathrm{tr}\left(\frac{J^T J}{2 \det J} \right) \tag{8}$$

where, J is the Jacobian of the transformation and ν is its Beltrami coefficient defined by [23]

$$\nu = \frac{\left| \frac{\partial w(z,\bar{z})}{\partial \bar{z}} \right|}{\left| \frac{\partial w(z,\bar{z})}{\partial z} \right|}. \tag{9}$$

In 2-D transformations, the condition for achieving conformal mapping is to meet the Cauchy-Riemann equations. In 3-D transformations, according to Liouville's theorem [24], only the Möbius transformations are conformal, which represent a hard limitation to achieve conformal mapping in 3-D. However, one could extend the polynomial inversion, trigonometric inversion, or LSM in order to approximate Möbius transformations in a similar way to what is presented here. Another solution that has been proposed for 3-D transformations is to simple extrude or revolve a 2-D refractive index profile [25].

The waveguides designed using quasi-conformal transformation optics, with current techniques to obtain gradient refractive index [26]–[30], adds another powerful tool to create waveguides circuits in Integrated Optics [31]. Furthermore, once the proposed strategies to reduce anisotropy meets the boundary conditions leading to continuous junctions, the waveguide circuit obtained with these strategies can be analyzed via Waveguide Circuit Theory [32]–[34].

2. Numerical Results

In order to compare the three anisotropy reduction strategies presented in the previous section, two waveguide devices were designed: a broadening S curve, and a 90° bend waveguide. In the S curve a Gaussian beam with wavelength 1550 nm is excited on bottom side of the device and it is guided towards the top side with a horizontal displacement of 3 μm to the right and 50% waist broadening. In the 90° bend structure, the Gaussian beam leaves the device at the right after an equivalent bend with a 7 μm radius. Both example waveguides have a 0.8 μm-core with refractive index of 2.0 surrounded on both sides by cladding layers with 0.8 μm and refractive index of 1.6. The outside is considered vacuum.

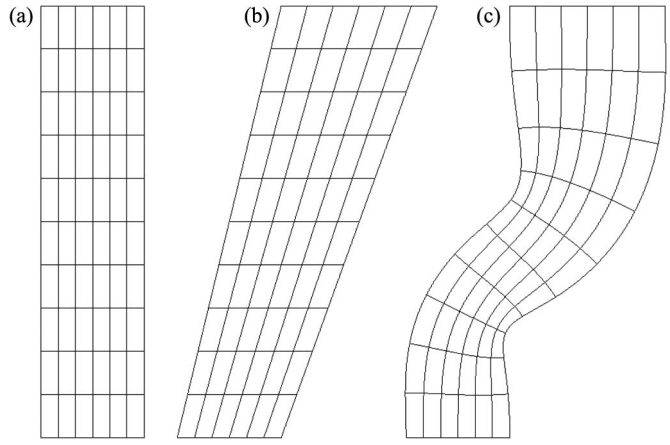

Fig. 1. Coordinate transformation for waveguide 1. (a) Original media. (b) Transformed media without anisotropy reduction (original transformation). (c) Transformed media with anisotropy reduction via the LSM with 36 degrees of freedom.

One possible starting coordinate transformation for the S curve is given by [17]

$$x' = 3\left(1 + \frac{xy}{20}\right)\left(\frac{y}{10}\right) + x\left(1 - \frac{y}{10}\right) + \sin\left(\frac{\pi y}{10}\right)P_x(x, y) \tag{10}$$

$$y' = y + \sin\left(\frac{\pi y}{10}\right)P_y(x, y) \tag{11}$$

with x and y in micrometers. The non-transformed medium is defined in region $-1.2\ \mu\text{m} \leq x \leq 1.2\ \mu\text{m}$ and $0 \leq y \leq 10\ \mu\text{m}$, as represented in Fig. 1(a). The beam is excited in the input position at $y = 0$ and the output is measured at $y = 10\ \mu\text{m}$. According to (5) and (6), b is chosen such that the perturbation functions P_x and P_y do not interfere with the device functionality, determined in this case by the transformation at the input and output boundaries. Thus, it was chosen of $b(x, y) = \sin(\pi y/10)$. The transformation with no perturbations is illustrated in Fig. 1(b), where the constant x and constant y curves on the $x'y'$-plane are plotted. Fig. 1(c) represents the optimized transformed medium with LSM.

As indicated earlier, the perturbation functions form depends on the anisotropy minimization strategy. In the case of polynomial inversion and the LSM, polynomial series in x and y were used:

$$P_x = \sum_{i=0}^{q}\sum_{j=0}^{p} A_{ij}x^i y^j \tag{12}$$

$$P_y = \sum_{i=0}^{q}\sum_{j=0}^{p} B_{ij}x^i y^j. \tag{13}$$

For the trigonometric inversion, we use

$$\begin{aligned} P_x = &\sum_{i=0}^{\left\lfloor\frac{q+1}{2}\right\rfloor}\sum_{j=0}^{\left\lfloor\frac{q+1}{2}\right\rfloor} A_{ij}\cos(ik_x x)\cos(jk_y y) + \sum_{i=0}^{\left\lfloor\frac{q+1}{2}\right\rfloor}\sum_{j=0}^{\left\lfloor\frac{p}{2}\right\rfloor} B_{ij}\cos(ik_x x)\sin(jk_y y) \\ &+ \sum_{i=0}^{\left\lfloor\frac{q}{2}\right\rfloor}\sum_{j=0}^{\left\lfloor\frac{q+1}{2}\right\rfloor} C_{ij}\sin(ik_x x)\cos(jk_y y) + \sum_{i=0}^{\left\lfloor\frac{q}{2}\right\rfloor}\sum_{j=0}^{\left\lfloor\frac{p}{2}\right\rfloor} D_{ij}\sin(ik_x x)\sin(jk_y y) \end{aligned} \tag{14}$$

$$\begin{aligned} P_y = &\sum_{i=0}^{\left\lfloor\frac{q+1}{2}\right\rfloor}\sum_{j=0}^{\left\lfloor\frac{q+1}{2}\right\rfloor} E_{ij}\cos(ik_x x)\cos(jk_y y) + \sum_{i=0}^{\left\lfloor\frac{q+1}{2}\right\rfloor}\sum_{j=0}^{\left\lfloor\frac{p}{2}\right\rfloor} F_{ij}\cos(ik_x x)\sin(jk_y y) \\ &+ \sum_{i=0}^{\left\lfloor\frac{q}{2}\right\rfloor}\sum_{j=0}^{\left\lfloor\frac{q+1}{2}\right\rfloor} G_{ij}\sin(ik_x x)\cos(jk_y y) + \sum_{i=0}^{\left\lfloor\frac{q}{2}\right\rfloor}\sum_{j=0}^{\left\lfloor\frac{p}{2}\right\rfloor} H_{ij}\sin(ik_x x)\sin(jk_y y) \end{aligned} \tag{15}$$

TABLE 1

Polynomial inversion results: maximum and mean anisotropy and maximum and minimum refractive index

p	q	DoF	$\max(K-1)$	$\text{avg}(K-1)$	$n_{\max}$	$n_{\min}$
–	–	0	0.1265333	0.0674598	1.927	1.392
0	0	1	0.0817237	0.0254140	2.483	1.124
1	1	4	0.0873881	0.0370300	2.284	1.066
2	2	9	0.0471612	0.0068671	2.482	1.061
3	2	12	0.0392501	0.0059338	2.529	1.070
3	3	16	0.0536650	0.0085786	2.617	1.065
4	3	20	0.0375948	0.0085786	2.428	1.037
4	4	25	0.0847293	0.0136693	2.681	1.010
5	4	30	0.0482167	0.0080072	2.745	1.023
5	5	36	0.0967206	0.0159214	2.831	1.079
6	5	42	0.6105765	0.0716793	3.031	1.035
7	5	48	2.4019314	0.6583801	2.854	1.031

TABLE 2

Trigonometric inversion results: maximum and mean anisotropy and maximum and minimum refractive index

p	q	DoF	$\max(K-1)$	$\text{avg}(K-1)$	$n_{\max}$	$n_{\min}$
–	–	0	0.1265333	0.0674598	1.927	1.392
0	0	1	0.0817237	0.0254140	2.483	1.124
1	1	4	0.0325561	0.0056183	2.566	1.083
2	2	9	0.0087056	0.0031507	2.765	1.052
3	2	12	0.0054852	0.0026594	2.702	1.048
3	3	16	0.0028040	0.0007946	2.491	1.039
4	3	20	0.0019573	0.0007946	2.562	1.037
4	4	25	0.0033280	0.0011209	2.800	1.031
5	4	30	0.0021413	0.0006122	2.507	1.036
5	5	36	0.0015735	0.0005347	2.731	1.035
6	5	42	0.0193402	0.0058214	3.178	1.405
7	5	48	0.1301982	0.0701956	2.915	1.384

where $k_x = 2\pi(x_{\max} - x_{\min})^{-1}$, and $k_y = 2\pi(y_{\max} - y_{\min})^{-1}$.

The three strategies were evaluated for different degrees of freedom in the perturbation functions. The sampling set was chosen according to the strategy: For both inversions, the set used was a $p \times q$ regular grid of points over the original domain; for the LSM, we used the adaptive algorithm detailed in [17], where the iterative sampling set choice is tuned to minimize the ratio between maximum and average anisotropies.

The interpolated anisotropy was evaluated in a much finer grid composed of 240×1000 points, aiming at a proper evaluation of the maximal anisotropy. The results are displayed in Tables 1–3 with the values for p, q, and the degrees of freedom (DoF) considered. The first line in all tables represents the original (unperturbed) transformation and it is the same among all strategies.

Fig. 2(a) compares the maximum anisotropy for all investigated strategies. It is clear that only the LSM is able to bring the residual anisotropy as close to zero as desired. The strategies using trigonometric and polynomial inversion are less effective and may even increase the maximum anisotropy above the original transformation when degrees of freedom of P_x and P_y increase past a certain optimal value due to high frequency oscillations in the interpolations.

TABLE 3

Least squares method results: maximum and mean anisotropy and maximum and minimum refractive index

p	q	DoF	$\max(K-1)$	$\text{avg}(K-1)$	$n_{\max}$	$n_{\min}$
–	–	0	0.1265333	0.0674598	1.927	1.392
0	0	1	0.0622339	0.0853228	2.243	1.190
1	1	4	0.0166739	0.0056183	2.341	1.046
2	2	9	0.0049703	0.0018600	2.482	1.029
3	2	12	0.0015915	0.0005519	2.510	1.006
3	3	16	0.0006393	0.0002160	2.592	1.018
4	3	20	0.0002599	0.0000899	2.970	1.037
4	4	25	0.0002000	0.0000713	3.124	1.032
5	4	30	0.0000321	0.0000111	3.405	1.030
5	5	36	0.0000275	0.0000092	3.644	1.042
6	5	42	0.0000117	0.0000039	4.347	1.037
7	5	48	0.0000013	0.0000005	5.148	1.031

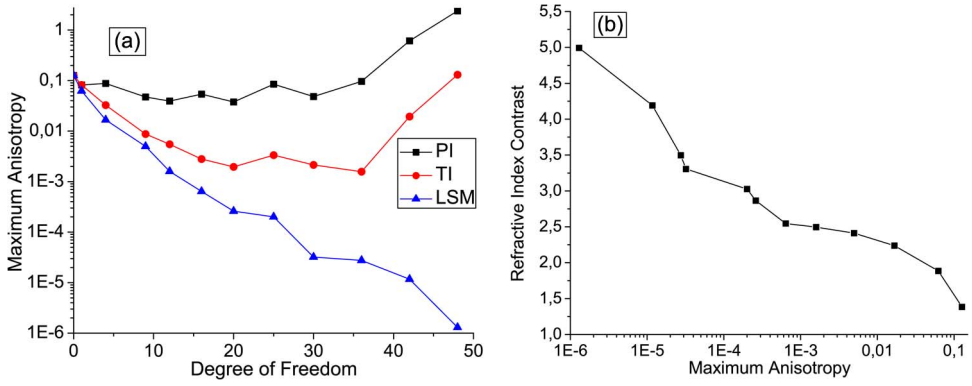

Fig. 2. Results of the minimization of residual anisotropy in the S curve. (a) Maximum anisotropy for the three methods applied with varying degrees of freedom in the transformation. (b) Compromise between acceptable residual maximum anisotropy and the required refractive index contrast in the resulting medium for the LSM strategy.

Nevertheless, the use of trigonometric functions gives much better results than polynomials and it is useful in this case if a maximum anisotropy on the order of 1% is acceptable, since it requires a much simpler implementation than the LSM. It is important to note that the choice of sampling points impacts the final transformation for the inversion strategies, but the same general conclusions hold. We also show the effect of the anisotropy reduction in the refractive index contrast (maximal to minimal index ratio) of the resulting medium for the LSM case in Fig. 2(b). This curve shows that the minimization of the residual anisotropy comes at the price of an increased index contrast requirement, which can also be an issue in the fabrication of these devices, although not as problematic as the anisotropy. Other works, such as [10], [11], [17], and [18], also resulted in increased refractive index contrast when anisotropy is reduced. We point out that neither the inversions nor the LSM strategies are able to not constraint the refractive index (or more precisely the index contrast) beforehand to predefined limits.

Both the original transformation and the LSM-optimized structure were simulated with 36 degrees of freedom—displayed in Fig. 1(b) and (c)—using the Finite Element Method in COMSOL Multiphysics to evaluate the wave propagation in the respective waveguides. In the simulation, the device media was considered isotropic, and therefore, any residual anisotropy from the transformations would result in deviations from the ideal wave propagation. The isotropic

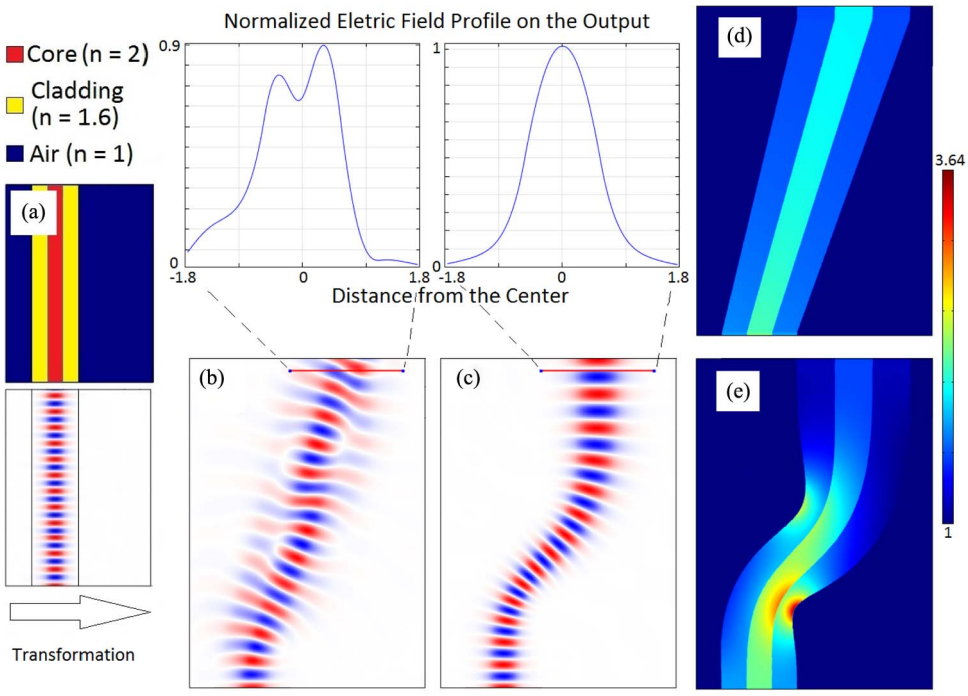

Fig. 3. Simulation results for the LSM optimization strategy applied to the S curve. (a) Original media. (b) Electric field distribution over the transformed device without anisotropy reduction. The cross-section plot shows the deformations in the Gaussian shape resulting from the anisotropy (not included in the simulation). (c) Electric field distribution for the device optimized with 36 degrees of freedom. The beam propagates through the structure virtually without distortions. (d) Refractive index distribution for the original transformation. (e) Refractive index distribution for the optimized media.

approximation is carried out by assuming a conformal transformation, for which the refractive index n' can be calculated by [10]

$$n'^2 = n^2 \cdot \frac{tr(J^T \cdot J)}{2det(J)^2} \tag{16}$$

where n is the refractive index of the original media.

These results are presented in Fig. 3, where the improvement in performance brought about by the anisotropy minimization is clear from both the electric field distributions and their cross-section at the outputs of the devices. There is no appreciable deviation from the initial Gaussian shape in the LSM case (apart of course from the intended 50% waist broadening).

In the case of the 90° bend, the original transformation is given by

$$x' = 7\frac{y}{10} + x\left(1 - \frac{y}{10}\right) + \sin\left(\frac{\pi y}{10}\right) P_x(x, y) \tag{17}$$

$$y' = (7 - x)\frac{y}{10} + \sin\left(\frac{\pi y}{10}\right) P_y(x, y) \tag{18}$$

and the results for maximum anisotropy for all three strategies are compiled in Table 4.

From the curves presented in Fig. 4(a) the difference in effectiveness of the LSM compared to the inversions is even more accentuated. Similar conclusions to the ones obtained from the S curve design can be drawn for this structure as well. While both inversion methods suffer from interpolation oscillations, the choice of trigonometric functions leads to a little less severe effects. Once again the relation between the required refractive index contrast and the residual maximum anisotropy in the optimized media reflects the compromise that must be achieved

TABLE 4

Maximum anisotropy for the 90° waveguide bend obtained by polynomial inversion (PI), trigonometric inversion (TI), and the LSM

p	q	DoF	PI	TI	LSM
–	–	0	0.4420690	0.4420689	0.4420689
0	0	1	0.1841500	0.1841500	0.1248781
1	1	4	0.1522152	0.1051256	0.0211005
2	2	9	0.1021757	0.0821484	0.0025803
3	2	12	0.0815432	0.0558428	0.0013940
3	3	16	0.2015894	0.0945841	0.0004689
4	3	20	0.1845327	0.0751295	0.0001484
4	4	25	0.2536151	0.0715234	0.0001252
5	4	30	0.3078506	0.0685142	0.0000220
5	5	36	0.9560215	0.0415635	0.0000182
6	5	42	1.5191201	0.2141544	0.0000071
7	5	48	3.1684327	0.4500085	0.0000009

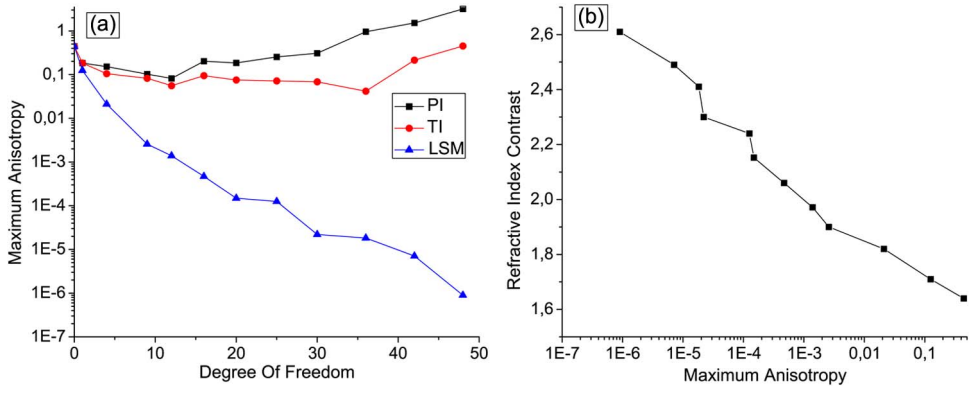

Fig. 4. Results of the minimization of residual anisotropy in the waveguide bend. (a) Maximum anisotropy for the three methods applied with varying degrees of freedom in the transformation. (b) Compromise between acceptable residual maximum anisotropy and the required refractive index contrast in the resulting medium for the LSM strategy.

according to specific fabrication capabilities and acceptable propagation deviations. It is also clear comparing these to the previous results that the exact values of index contrast strongly depend on the original transformation and must be evaluated for each new design.

The Fig. 5 show the numerical simulation results for the 90° bend. These results lead to similar conclusions to those drawn from the S curve in Fig. 3.

In both waveguides the ignored residual anisotropy leads to scattering with different patterns for different polarizations, with transmissions never greater than −1.5 dB. On the other hand, for both waveguides with reduced anisotropy, the insertion losses in simulation are negligible for any polarization, since the electromagnetic field distributions are almost perfectly preserved. These results confirm the anisotropy reduction effectiveness in the waveguide performance.

3. Conclusion

This work presented a comparison between strategies for minimization of residual anisotropy in quasi-conformal mappings for transformation optics designs. We showed that the LSM has a clear advantage over the faster inversion methods with polynomial and trigonometric basis functions. Nevertheless, due to simplicity, there are cases where the inversion with trigonometric functions might result in an acceptable solution as long as the high-frequency oscillations in the

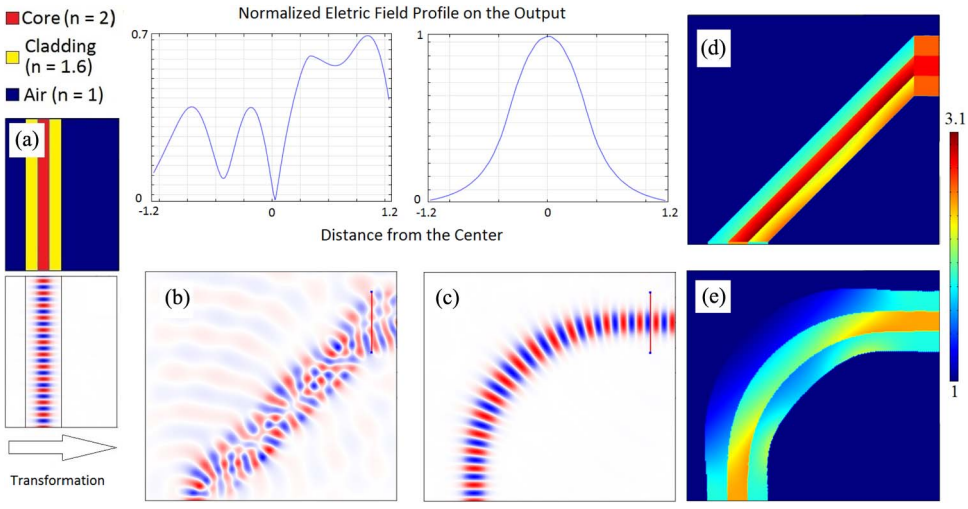

Fig. 5. Simulation results for the LSM optimization strategy applied to the waveguide bend. (a) Original media. (b) Electric field distribution over the transformed device without anisotropy reduction. The cross-section plot shows the deformations in the Gaussian shape resulting from the anisotropy (not included in the simulation). (c) Electric field distribution for the device optimized with 36 degrees of freedom. The beam propagates through the structure virtually without distortions. (d) Refractive index distribution for the original transformation. (e) Refractive index distribution for the optimized media.

final interpolation are avoided. Two design examples were used to validate and compare the techniques presented over a wide range of conditions. We have also shown how the minimization of the residual anisotropy generally leads to higher requirements of refractive index contrast, a compromise that has to be taken into account considering the fabrication capabilities available.

References

[1] U. Leonhardt, "Optical conformal mapping," *Science*, vol. 312, no. 5781, pp. 1777–1780, Jun. 2006.
[2] J. B. Pendry, D. Schurig, and D. R. Smith, "Controlling electromagnetic fields," *Science*, vol. 312, no. 5781, p. 1780–1782, 2006.
[3] U. Leonhardt and T. G. Philbin, "General relativity in electrical engineering," *New J. Phys.*, vol. 8, no. 10, p. 247, Oct. 2006.
[4] N. Kundtz, D. Smith, and J. Pendry, "Electromagnetic design with transformation optics," *Proc. IEEE*, vol. 99, no. 10, pp. 1622–1633, Oct. 2011.
[5] U. Leonhardt and T. G. Philbin, "Transformation optics and the geometry of light," ArXiv e-prints, May 2008.
[6] L. Ahlfors, *Lectures on Quasiconformal Mappings*. Providence, RI, USA: AMS, 1966, ser. University Lecture Series.
[7] J. Li and J. B. Pendry, "Hiding under the carpet: A new strategy for cloaking," *Phys. Rev. Lett.*, vol. 101, no. 20, p. 203901, Nov. 2008.
[8] U. Leonhardt and T. Philbin, *Geometry and Light: The Science of Invisibility*. New York, NY, USA: Dover, 2010.
[9] G. Shilov, *Elementary Real and Complex Analysis*. New York, NY, USA: Dover, 1996, ser. Dover Books on Mathematics.
[10] D. Liu, L. H. Gabrielli, M. Lipson, and S. G. Johnson, "Transformation inverse design," *Opt. Exp.*, vol. 21, no. 12, pp. 14 223–14 243, Jun. 2013.
[11] Z. Chang, X. Zhou, J. Hu, and G. Hu, "Design method for quasi-isotropic transformation materials based on inverse Laplace's equation with sliding boundaries," *Opt. Exp.*, vol. 18, no. 6, pp. 6089–6096, Mar. 2010.
[12] W. Tang, C. Argyropoulos, E. Kallos, W. Song, and Y. Hao, "Discrete coordinate transformation for designing all-dielectric flat antennas," *IEEE Trans. Antennas Propag.*, vol. 58, no. 12, pp. 3795–3804, Dec. 2010.
[13] C. Mateo-Segura, A. Dyke, H. Dyke, S. Haq, and Y. Hao, "Flat Luneburg lens via transformation optics for directive antenna applications," *IEEE Trans. Antennas Propag.*, vol. 62, no. 4, pp. 1945–1953, Apr. 2014.
[14] D.-H. Kwon, "Quasi-conformal transformation optics lenses for conformal arrays," *IEEE Antennas Wireless Propag. Lett.*, vol. 11, pp. 1125–1128, 2012.
[15] I. Aghanejad, H. Abiri, and A. Yahaghi, "Design of high-gain lens antenna by gradient-index metamaterials using transformation optics," *IEEE Trans. Antennas Propag.*, vol. 60, no. 9, pp. 4074–4081, Sep. 2012.
[16] Q. Wu *et al.*, "Transformation optics inspired multibeam lens antennas for broadband directive radiation," *IEEE Trans. Antennas Propag.*, vol. 61, no. 12, pp. 5910–5922, Dec. 2013.

[17] M. A. F. C. Junqueira, L. H. Gabrielli, and D. H. Spadoti, "Anisotropy minimization via least squares method for transformation optics," *Opt. Exp.*, vol. 22, no. 15, pp. 18 490–18 498, Jul. 2014.
[18] N. I. Landy and W. J. Padilla, "Guiding light with conformal transformations," *Opt. Exp.*, vol. 17, no. 17, pp. 14 872–14 879, Aug. 2009.
[19] C. García-Meca *et al.*, "Squeezing and expanding light without reflections via transformation optics," *Opt. Exp.*, vol. 19, no. 4, pp. 3562–3575, Feb. 2011.
[20] R. Yang, Z. Lei, L. Chen, Z. Wang, and Y. Hao, "Surface wave transformation lens antennas," *IEEE Trans. Antennas Propag.*, vol. 62, no. 2, pp. 973–977, Feb. 2014.
[21] P. Zhang, Y. Jin, and S. He, "Inverse transformation optics and reflection analysis for two-dimensional finite-embedded coordinate transformation," *IEEE J. Sel. Topics Quantum Electron.*, vol. 16, no. 2, pp. 427–432, Mar. 2010.
[22] W. Yan, M. Yan, and M. Qiu, "Necessary and sufficient conditions for reflectionless transformation media in an isotropic and homogenous background," ArXiv e-prints, Jun. 2008.
[23] K. Astala, T. Iwaniec, and G. Martin, *Elliptic Partial Differential Equations and Quasiconformal Mappings in the Plane (PMS-48)*. Princeton, NJ, USA: Princeton Univ. Press, 2008, ser. Princeton Mathematical Series.
[24] D. E. Blair, *Inversion Theory and Conformal Mapping*. Providence, RI, USA: AMS, 2000.
[25] N. Kundtz and D. R. Smith, "Extreme-angle broadband metamaterial lens," *Nature Mater.*, vol. 9, no. 2, pp. 129–132, Feb. 2010.
[26] U. Levy *et al.*, "Implementation of a graded-index medium by use of subwavelength structures with graded fill factor," *J. Opt. Soc. Amer. A Opt. Image Sci. Vis.*, vol. 22, no. 4, pp. 724–733, Apr. 2005.
[27] D. H. Spadoti, L. H. Gabrielli, C. B. Poitras, and M. Lipson, "Focusing light in a curved-space," *Opt. Express*, vol. 18, no. 3, pp. 3181–3186, Feb. 2010.
[28] L. H. Gabrielli, J. Cardenas, C. B. Poitras, and M. Lipson, "Silicon nanostructure cloak operating at optical frequencies," *Nature Photon.*, vol. 3, pp. 461–463, Aug. 2009.
[29] D. Beltrami *et al.*, "Planar graded-index (GRIN) PECVD lens," *Electron. Lett.*, vol. 32, no. 6, pp. 549–550, Mar. 1996.
[30] M. Yin, X. Yong Tian, L. Ling Wu, and D. Chen Li, "All-dielectric three-dimensional broadband Eaton lens with large refractive index range," *Appl. Phys. Lett.*, vol. 104, no. 9, 2014, Art. ID. 094101.
[31] R. Hunsperger, *Integrated Optics: Theory and Technology*, 6th ed. New York, NY, USA: Springer-Verlag, Apr. 2009.
[32] D. M. Kerns and R. W. Beatty, *Basic Theory of Waveguide Junctions and Introductory Microwave Network Analysis*, 1st ed. London, U.K.: Pergamon Press, Apr. 1967.
[33] R. B. Marks and D. F. Williams, "A general waveguide circuit theory," *J. Res. Nat. Inst. Stand. Technol.*, vol. 97, no. 5, pp. 533–562, Sep./Oct. 1992.
[34] D. Williams and B. Alpert, "Causality and waveguide circuit theory," *IEEE Trans. Microw. Theory Techn.*, vol. 49, no. 4, pp. 615–623, Apr. 2001.